Vietnam Journal of Science and Technology ***58*** *(4) (2020) 481-492*

doi:10.15625/2525-2518/58/4/15034

REALIZATION OF BROADBAND AND INDEPENDENT POLARIZATION METAMATERIAL PERFECT ABSORBER BASED ON THE THIRD-ORDER RESONANCE

Nguyen Thi Hien[1, *], Phan Thi Duyen[2], Bui Xuan Khuyen[2], Bui Son Tung[2], Nguyen Xuan Ca[1], Phạm Thị Thu Ha[1], Vu Dinh Lam[3]

[1]*Faculty of Physics and Technology, TNU- University of Sciences, Tan Thinh Ward, Thai Nguyen city, Viet Nam*

[2]*Institute of Materials Science, VAST, 18 Hoang Quoc Viet, Cau Giay, Ha Noi, Viet Nam*

[3]*Graduate University of Science and Technology, VAST, 18 Hoang Quoc Viet, Cau Giay, Ha Noi, Viet Nam*

[*]Email: *hiennt@tnus.edu.vn*

Received: 4 May 2020; Accepted for publication: 20 June 2020

Abstract. Since the first observation of the fascinating absorption property, metamaterials have been become a scientific spotlight. A distinctive interest has been given to metamaterial absorber (MA) with a broad operating band, which are more useful for future applications. In this report, we studied numerically and experimentally the electromagnetic properties of perfect MAs using ring-shaped structures at microwave frequencies. By creating a magnetic resonance, the ring structure confines electromagnetic energy at the first- and third-order resonances. And then, we leveraged the super-cell structures, which consist of different rings in one unit cell to obtain broadband absorption. The results showed that the absorption band of MA is broaden from 1.3 to 2.17 GHz when the number of rings in the unit cell increases from four to nine-rings. The experiment results are in good agreement with the simulation ones. Finally, by applying the same model, we simulated the MA working at THz frequency. Especially, all GHz- and THz-MAs are optimized by the third-order magnetic resonance, which occurs at a frequency three times higher than the fundamental resonance one.

Keywords: metamaterials, broadband, perfect absorption, third-order resonance.

Classification numbers: 2.1.2, 2.10.1.

1. INTRODUCTION

Over the past decade, a new class of artificial materials, the so-called metamaterials (MMs), have shown many unusual properties, which are not found in natural materials, such as materials with simultaneously negative permittivity and permeability leading to negative refractive index [1 - 5] and numerous fascinating applications such as the perfect lens [6], the invisible cloaking [7, 8], and the electromagnetically-induced transparency [9, 10]. Recently,

the applicability of MMs as electromagnetic-wave absorption has been attracted the interest of many scientists from the viewpoint of feasible MM applications using current technology. A near-unity absorber is a device in which all incident radiation is completely consumed at a specific frequency. Consequently, the transmission, the reflection and all other light propagation channels are unable [11 - 13]. Electromagnetic wave absorbers can be used in devices and areas such as: emitters [14 - 16], sensors [17], spatial light modulators [18], IR camouflage [19], thermophotovoltaics, and wireless communication [20]. The first perfect absorber (PA) has been demonstrated under the concept of MMs at GHz regime by Landy *et al.* [21]. By modulating the imaginary part of refractive index and the impedance $Z(\omega)$ of MM, a near-unity absorption peak can be realized at the resonant frequency. Up to date, PA has been demonstrated in every technologically relevant spectral ranges, from microwave [12, 13, 22], THz [17, 23], NIR [24], to the near optical [25]. For different applications, the MM absorbers (MAs) have been achieved in narrow peak [17, 21, 23, 26], multi-band peaks [13, 27], and broadband [22, 28]. The multi-peak and broadband MAs have been observed by two configurations, arranging appropriately unit cells of PA peak [29, 30] and using the multi-layer model of absorption [31]. It notices that there are many interactions between plasmons in the configurations. Hence, it is a problem to combine broadband MAs with high efficiency, since the sensitive PA conditions are easy to be broken by these interactions. Therefore, the achievement of narrow peak, multi-peak, and broadband absorption which deal with different applications are still the significant issue in the MM researches. Other side, most recent studies show that the MM absorption mechanism is due to the fundamental magnetic or the electrical resonance [11-13, 27-30], where their unit-cell size must be much smaller than the operating wavelength. This will be difficult to manufacture especially when operating in the high-frequency region.

In our paper, firstly, a high symmetric MA was designed to operate at the GHz and the THz range. Our results show that a PA peak was not only achieved at the fundamental magnetic resonance frequency but also at the third-order magnetic resonant frequency, which occurs at a frequency three times higher than the one. And then, we used the super cell structures, which consist of several rings with difference size in one-unit cell, we got the broadband MMs absorber. The result shows that the absorption bandwidth can be increased by changing number of rings in the unit cell. The experiment results are quite coincident with the simulated ones. Finally, based on the initial MA, a THz-MA is designed and characterized for further applications.

2. SIMULATION AND EXPERIMENT

The simulation was carried out by using a finite-integration technique package of CST Studio. For a single peak of absorption at the third-order asymmetric resonance frequency, the conventional absorber design, sandwich model: layer1–layer2–layer3, was employed to investigate the absorptions. The front layer that is arranged periodically by metallic rings and the back one that is metallic plane are separated by a dielectric layer. The conductor is copper with an electric conductivity of 5.96×10^7 S/m. The dielectric is FR-4 with a relative dielectric constant of 4.3 and a loss-tangent of 0.025 (agree with the real PCB substrates) [30]. A unit cell of the MA was shown in Fig. 1(a). The geometrical parameters are set to be a = 18 mm, R_1 = 8.2 mm, R_2 = 2 mm. The thickness of copper layer is t_s = 0.036 mm. The MA was designed to work in the range of 12–18 GHz. The EM wave is polarized in such a way that the electric and the magnetic fields are parallel with the MM slab, while the wave vector k propagates normally to the front side of the MA (Fig. 1 (a)). The boundary conditions are set so that the unit cells are

periodic in the E–H plane. The environment in the simulations is defined as free space which corresponds with the experimental method. In the conventional absorber model, the back layer is the EM-wave-prevented plane. The absorption A(ω) is calculated through $A(\omega) = 1 - R(\omega) - T(\omega) = 1 - |S_{11}|^2 - |S_{21}|^2$, where the reflection $R(\omega) = |S_{11}|^2$, and the transmission $T(\omega) = |S_{21}|^2$.

The fabricated samples were made in a cleanroom by using the photolithography technique. The printed-circuit-board slabs were employed, whose parameters were coincident with the simulated optimizations. Fabricated prototype and measurement setup of the proposed structure are indicated in Figs. 1(b) and 1(c), respectively. The samples were measured in free space, using a Hewlett-Packard E8362B network analyzer connected to microwave standard-gain horn antennas. The operating range of EM wave was tested from 12 to 18 GHz.

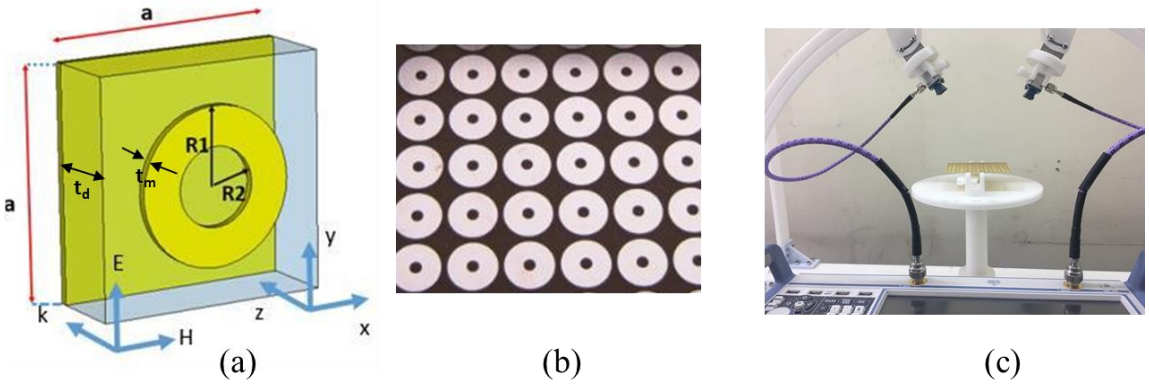

Figure 1. (a) Unit cells for a single peak of absorption, (b) fabricated sample, and (c) measurement set up for all the proposed structures (uniform and non-uniform ring-shaped).

3. RESUTLS AND DISCUSSION

3.1. Absorption behavior at GHz frequency

3.1. 1. Perfect metamaterial absorber based on ring structure

Currently, there is a number of perfect absorption structures that have been used, but there are some existing restrictions due to their complex structure and the difficult fabrication, especially in the optical region [25, 32] or polarization dependence [21]. To overcome the above disadvantages, we designed a simple structure with high symmetry, the so-called ring structure. In general, a unity absorption can be possibly achieved at certain frequency by canceling both reflection and transmission to be zero. The minimum reflection can be obtained by matching the impedance of the sample to the air at resonance frequency. However, the transmission is zero, since the copper film acts as a physical barrier to block the incident waves. Figure 2(a) shows simulated results of reflectance, transmittance and absorbance of PA using ring structure with two absorber peaks. The first absorbance peak is observed at f_1 = 4.67 GHz with absorption of 90 %, no transmission and reflection of 0.1 %. Especially, the second one is excited at f_3 = 13.8 GHz with absorption of 100 %, no transmission and no reflection. Besides, the influence of electromagnetic polarization on the absorption is examined in Fig. 2(b). It is shown that the polarization of the normal incident wave does not affect the absorption spectrum. The absorptions and peak position at 4.67 GHz and 13.8 GHz are unchanged since the polarization

angle is increased from 0° to 90°. The result can be explained due to the symmetry of the absorber in the E-H plane and it is an outstanding advantage of this structure.

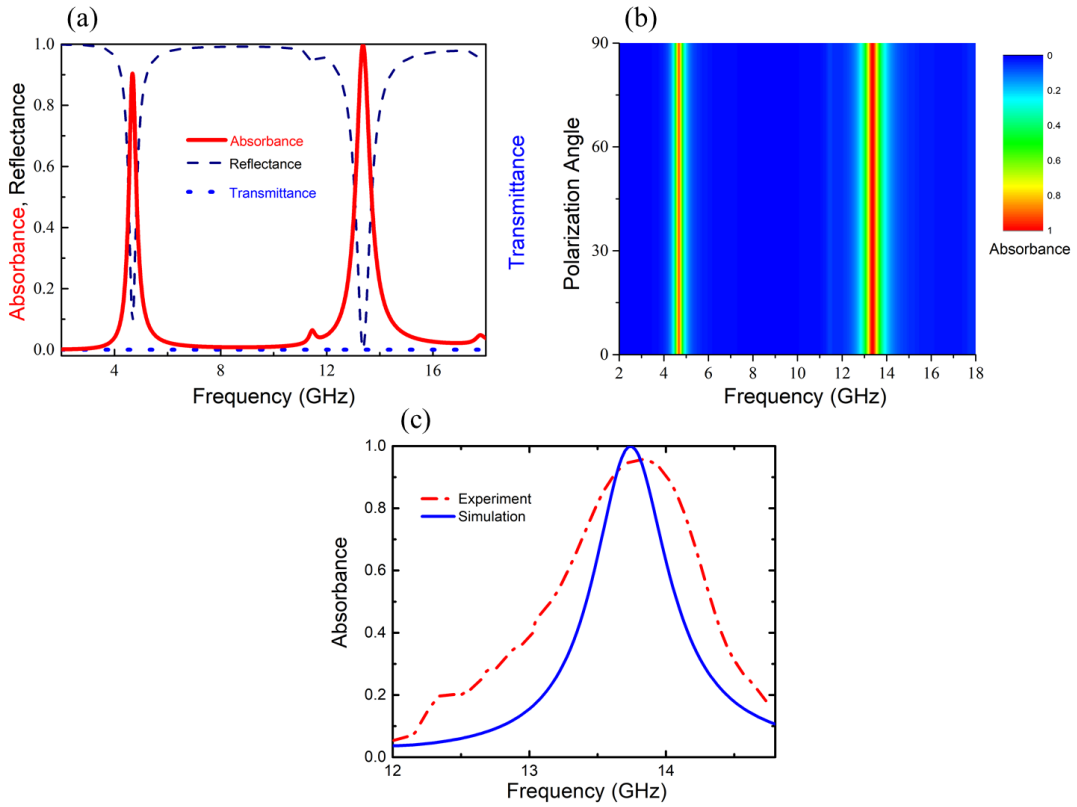

Figure 2. (a) Simulated results of reflectance, transmittance and absorbance. (b) Absorption spectra according to the polarization angle of the incident wave. (c) Simulated and experimental absorption spectrum at f_3 = 13.8 GHz.

Interestingly, at the same unit-cell size, the frequency f_3 has higher magnitude and lies at position of three times longer than that of f_1. So, the use of f_3 to create absolute absorption will make the fabrication of MPAs to be easier, especially at high-frequency. Because of this advantage, we only focus on the third-resonant magnetic frequency. Figure 2(c) shows the simulation and experiment spectrum of ring-structure at f_3 = 13.8 GHz. Clearly, the simulation and experiment results are quite agreement. The small discrepancies can be caused by the errors in fabrication and it may be due to the effect of the noise during the measurement process.

For further understanding these two absorption peaks, the surface-current distributions of the ring-shaped structure are simulated at f_1 = 4.67 GHz and f_3 = 13.8 GHz, as shown in Fig. 3. Figure 3(a) shows that there are only the anti-parallel currents on surfaces of ring and metal film which appear in the front layer of copper and the back of the sample. The currents flow in opposite directions to creating an induction magnetic field in the opposite direction with an external magnetic field. The interaction of the magnetic field induction and the external magnetic field caused fundamental magnetic resonance at 4.67 GHz frequency. This is first-order magnetic resonance [33, 34]. However, from the current distribution at 13.8 GHz, the magnetic response is not as simple as in the fundamental mode at 4.67 GHz. The surface current

in Fig. 3 (b) at 13.8 GHz shows that the induced magnetic moments concentrated mainly in the centers of three circular currents but in different directions since the central circular current is opposite to the others. It means that the resonance appears at f_3 is the third-order magnetic resonance [33, 34]. Further simulations (not shown here) also confirm the existence of higher odd modes (such as fifth, seventh, etc. order magnetic resonance). The even magnetic modes might not exist since the antiparallel induced magnetic fields cancel each other.

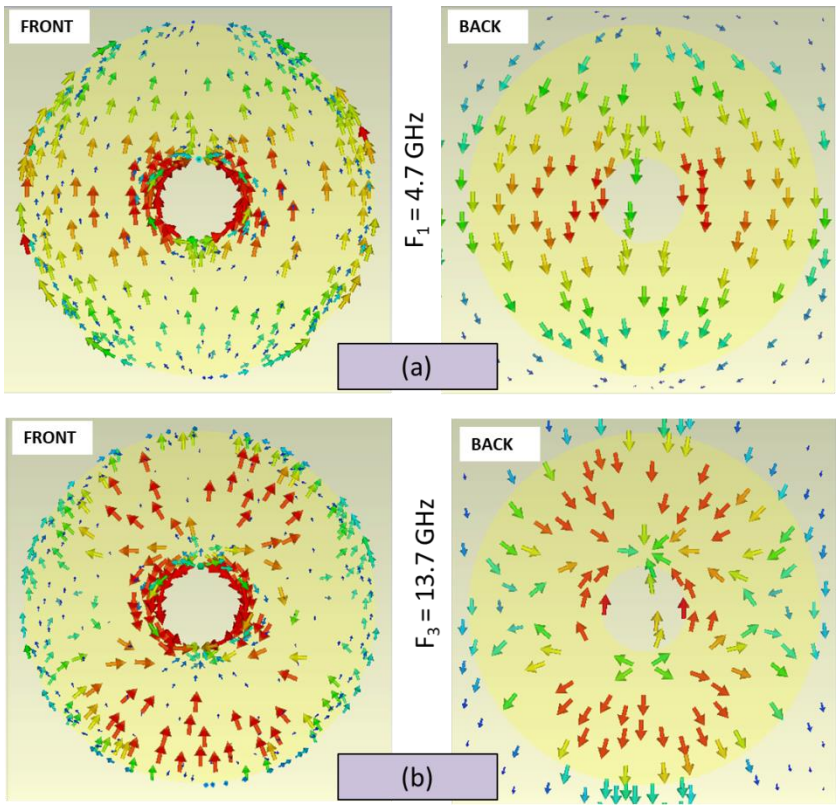

*Figure **3**.* The induced surface current distribution of single ring structure at: (a) f_1 = 4.7 GHz and (b) f_3 = 13.7 GHz.

With the ring-structure base on the third-order magnetic resonance, the above research results show that a perfect absorption has been achieved with the advantages of significant size for fabrication. However, due to resonant properties the absorption bandwidth is too narrow to be satisfy for more practical applications. Therefore, the next PA structure with high/broad band absorption is essential. The first method utilizes multiple resonating structures in each unit cell, exploiting the resonators with different sizes resonating at different frequencies. By combining them in one-unit cell, multiple resonances will appear in the absorption spectrum. If these absorption resonances are close enough in frequency, they will form a broadband absorption. Another method is stacking multiple layers in which resonators share the same ground plane, but the fabrication is not really easy [35]. Another method utilizes the different sections of a single structure that resonate at different frequencies to obtain multiple resonances [36]. However, the existing obstacle is the polarization sensitivity. Recently, another approach to realize broadband absorption, that is incorporating lumped elements into the MM resonators, seems to have been a

promising way for microwave frequencies [27]. Although adding lumped elements is an interesting idea, the feasibility in high frequency ranges such as near IR or optical region is still a problem due to the small size of MM resonator [37]. In this study, we propose, simulate and experiment an absorber MMs operating at a wide frequency band at the third-order resonance frequency by the first way utilizes multiple ring structures in each unit cell.

3.1.2. Perfect metamaterial absorber based on four - rings structure

First of all, in order to create a broadband absorber, we arranged four rings with different sizes at the front side of one-unit cell, the back one that is still metallic plane, as shown in Fig. 4(a). The unit cell of PA_1-structure with the structural parameters: a = 18 mm, t_m = 0.036 mm, R = 7.8 mm, R_{01} = 1.3 mm, R_1 = 7.4 mm, R_{11} = 2 mm, R_2 = 7.0 mm, R_{22} = 2.8 mm, R_3 = 6.6 mm, R_{33} = 2.5 mm, and t_d = 1.6 mm.

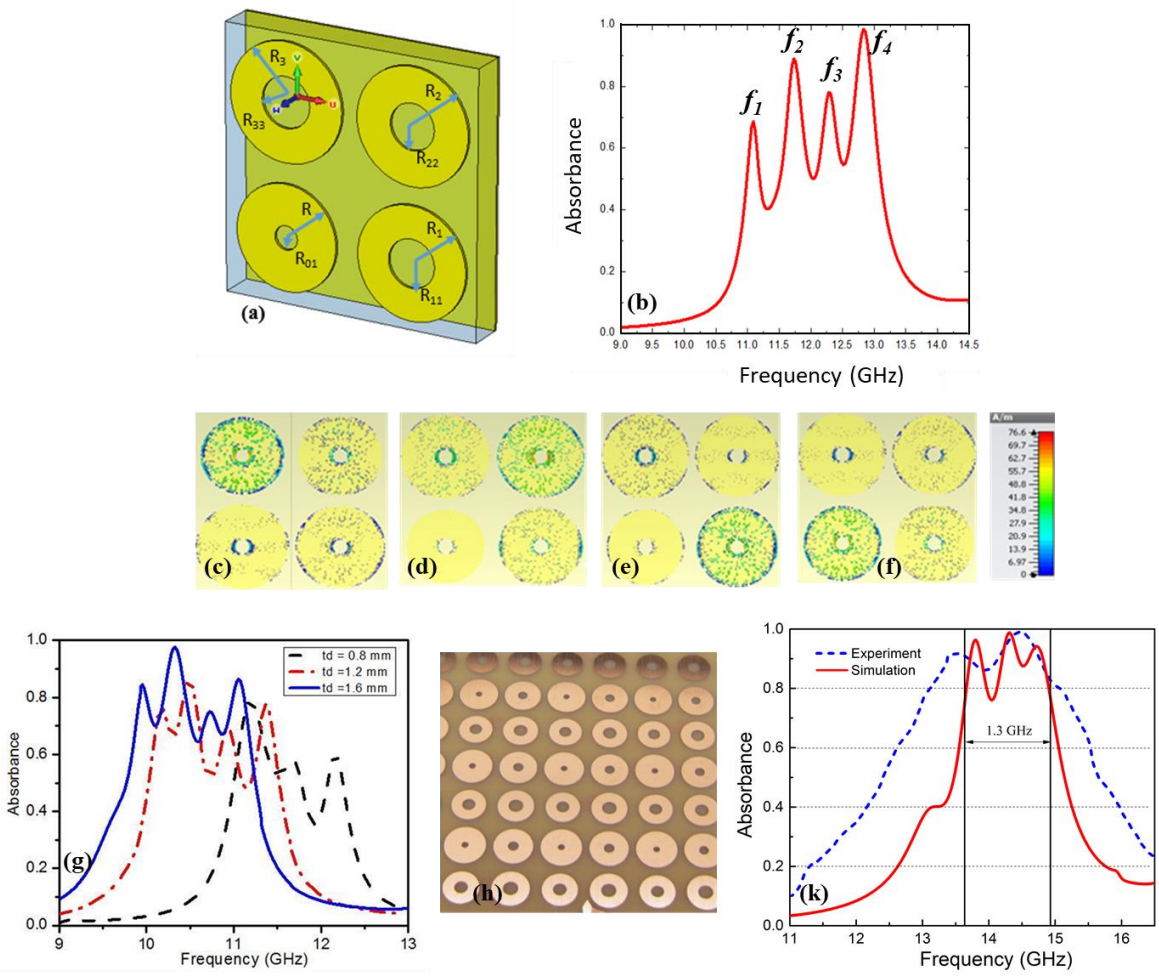

Figure 4. Four-ring structure designated as PA_1 with (a) super cell, (b) Simulated absorption spectrum. Surface current distribution at (c) f_1 = 10.79 GHz, (d) f_2 = 11.105 GHz, (e) f_3 = 11.574 GHz, and (f) f_4 = 12.03 GHz. (g) The absorption spectrum of the four-rings structure at third-order resonance

when the dielectric thickness changes. (h) Fabricated sample and (k) comparison between simulated and experimental absorption spectrum.

The Fig. 4(b) is presenting the simulated absorption spectrum of PA_1 based on the super cell with four-rings. The result shows that peaks at f_1 = 10.79 GHz, f_2 = 11.105 GHz, f_3 = 11.574 GHz, f_4 = 12.03 GHz are individually excited by different rings. The induced magnetic field distributions at these frequencies are shown in Fig. 4(c) to better understand the physics of the proposed multi-band absorption of the PA_1. It is obvious that, at a certain frequency, the magnetic field is localized and enhanced at some ring in the unit cell. At higher frequency, the magnetic field is localized at the ring with less radius and vice versa. This obtained results can be theoretically explained by using the LC circuit model and in full agreement with the results of the research in Ref. [38]. Besides, the magnetic field distributions in Fig. 4(c) also proves that the resonances appeared at all frequency are the third-order magnetic resonance. Like a ring - structure above, the induced magnetic moments also concentrated mainly in the centers of three circular currents but in different directions. This is the difference in this study compared to previous studies creating multi or broadband absorption [13, 20, 25, 27 - 30], which are derived from fundamental magnetic resonance.

Besides, we also studied the effect of dielectric thickness on the absorption. The results are shown in Fig. 4(g). Considering our current fabrication condition, we just studied the changing of dielectric thickness layer from 0.8 mm to 1.6 mm. It indicates that the absorption has strongly affected by the thickness of the dielectric layer. When the dielectric film thickness is increasing, the absorbance increases and the highest absorbance is obtained when t_d = 1.6 mm.

In order to obtain the broadband absorption, one of the most important issues is to shift the absorption frequencies close together. As shown in the Fig. 4 (b) and 4(g), the absorption frequency depends strongly on the radius of the ring and the highest absorbance is obtained when t_d = 1.6 mm. So, we have changed the value of the size of rings and fix t_d =1.6 mm to create the broadband MA. Finally, we obtained the broadband MAs with the structural parameters as: a = 18 mm, t_m = 0.036 mm, R = 7.6 mm, R_{01} = 1.3 mm, R_1 = 7.4 mm, R_{11} = 2 mm, R_2 = 7.2 mm, R_{22} = 2.8 mm, R_3 = 6.9 mm, R_{33} = 2.5 mm, t_d = 1.6 mm. Fabricated sample and the simulated and experimental absorption spectra of the optimized broadband MA based on four-rings structure shows in Fig. 4 (h) and (k), respectively. The result shows that an absorption over 85 % is achieved within a bandwidth of 1.3 GHz. The highest absorber in this range is 99 % at 14.32 GHz. The simulation and experiment results are good agreement, bandwidth absorber in experiment is broader than in simulation. Insignificant difference between simulation and experiment comes from a bit error in both fabrication and measurement.

3.1. 3. Perfect metamaterial absorber based on nine - rings structure

In order to widen the absorption bandwidth, we continue to optimize the super cell with nine-rings. As presented in Fig. 5(a), the structural parameters are elevated as follows: R = 7.8 mm, R_1 = 7.4 mm, R_2 = 7.0 mm, R_3 = 6.6 mm, R_4 = 7.8 mm, R_5 = 3.5 mm, R_6 = 6.7 mm, R_8 = 5.3 mm, R_{01} = R_{11} = R_{66} = 2 mm, R_{22} = 2.8 mm, R_{33} = 2.5 mm, R_{44} = 1.3 mm, R_{55} = 1 mm, R_{77} = 2.5 mm, R_{88} = 3 mm, a = 26 mm, t_d = 1.6 mm, and t_m = 0.036 mm. Fabricated sample and their simulated and experimental absorption spectra is shown in Fig. 5(b) and 5(c), respectively. The results show that we obtain the bandwidth absorber to 2.17 GHz with the average absorption of 85%. It is much broader comparing with the unit cell consisting of four-rings. The simulation and experiment results quite coincide with each other. The small discrepancies can be caused by the errors in manufacturing and also the noise in the measurement process.

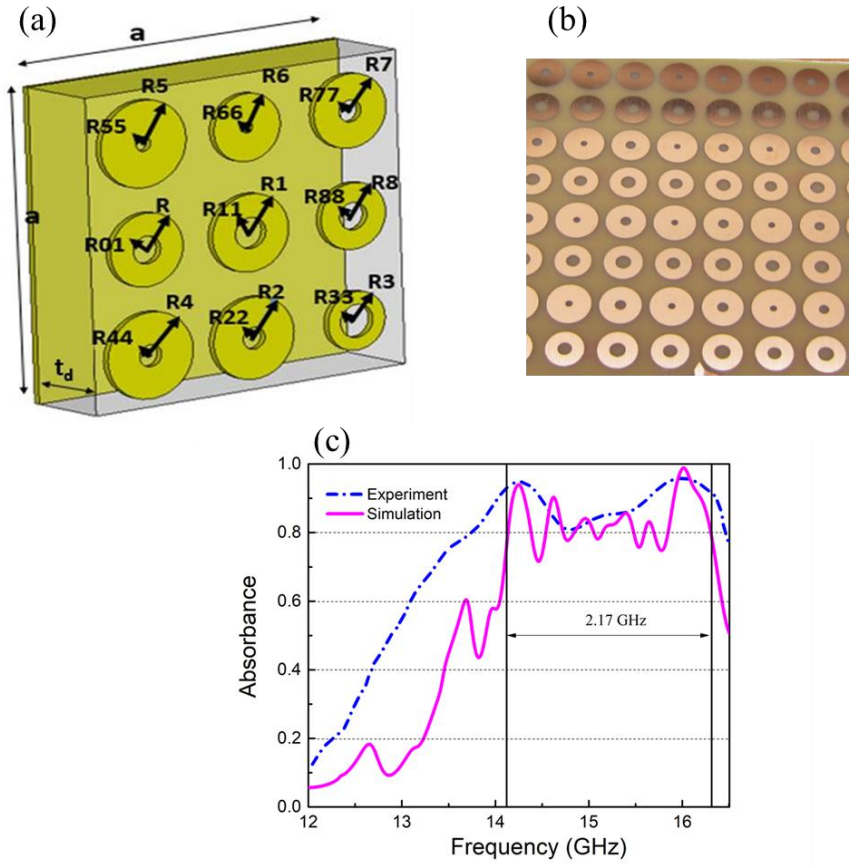

Figure 5. Nine- rings structure is demonstrated by (a) the unit cell, (b) fabricated sample and (c) the experimental and simulated absorption spectrum of nine-rings structure.

3.2. Absorption behavior at THz frequency

In addition to the potential applications in the microwave regime, broadband MAs at terahertz frequencies are attractive [39, 28], but at the same time challenging to construct. Therefore, MMs can replace the natural materials in the applications where the natural materials have not satisfied. A general approach to obtain the optical counterpart of the microwave PA is to scale down all geometrical parameters of the microwave designs. However, at high frequencies, the small unit cell becomes to be quite difficult for fabrication technologies. The third-order research shows that the unit-cell size increases significantly (about three times) compared to that at the first-order resonance. It can be further useful for the practical manufactures. From this motivation, a THz-MA is developed in this part.

From the initial single ring-shaped structure, we optimized the third-resonance of this structure in the THz frequency range. The parameters were designed as a = 75 μm, t_d = 2 μm, t_s = 0.18 μm, R_1 = 30 μm, and R_2 = 10 μm. The metal of structure was selected to be silver (Ag) with an electric conductivity of 6.3012 × 10^7 S/m. For simplicity, no substrate has been considered in the simulations. The dielectric constant of the dielectric spacer is unchanged. The absorption result and surface current distribution are presented in Fig. 6, where the third-order

absorption also excited at 3.5 THz. This resonance is also due to the magnetic resonance [see the anti-parallel surface currents at absorption peak, as simulated in Fig. 6 (b)].

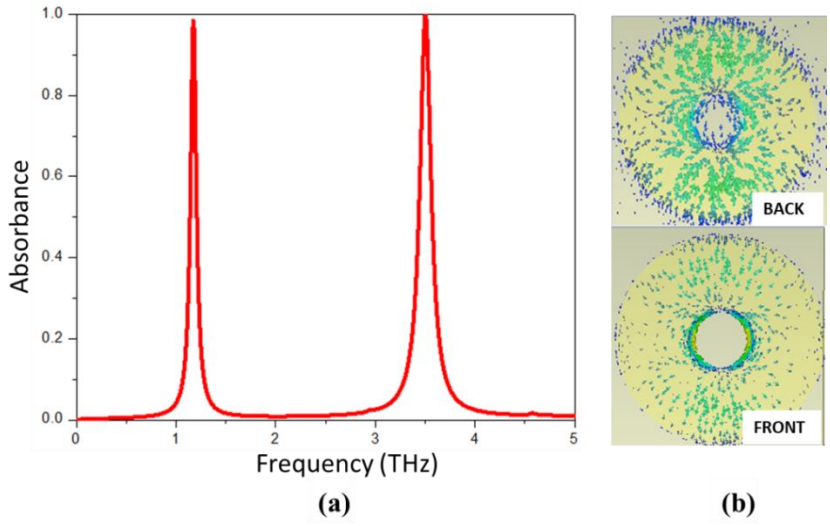

Figure 6. (a) Simulated absorption spectrum based on third-resonance of the single ring-shaped structure at THz frequency absorption spectrum. (b) Distribution of surface current at 3.5 THz.

We also investigated the broadband MPAs based on four-rings and nine-rings structure. In these simulations, all the sizes mentioned in 3.1.2 and 3.1.3 are shrank down simultaneously by a factor of 0.001. For simplicity, no substrate has been considered in the simulations. The dielectric constant of the dielectric spacer is unchanged. The absorption spectra are presented in Fig. 7(a) and 7(b). Clearly that the absorber width of four-rings and nine-rings are corresponding to 1.31 THz and 2.19 THz with absorbing over 80 %. These results would be useful for further experimental realizations of broadband absorber MMs and their applications at the THz frequency.

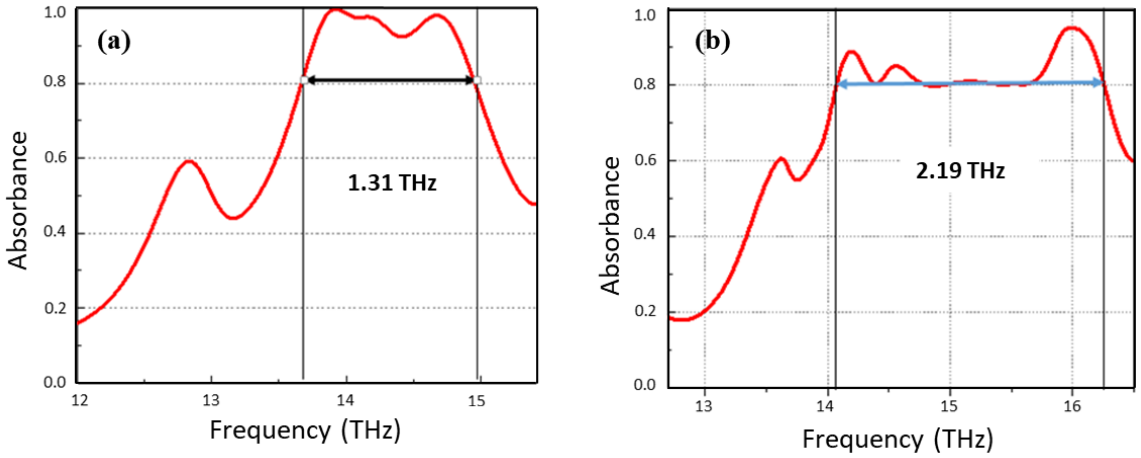

Figure 7. Broadband absorption spectrum of (a) four-rings and (b) nine-rings structure at the THz frequency.

4. CONCLUSION

In the microwave region, we studied numerically and experimentally the electromagnetic properties of perfect MAs using ring-shaped structures. It is shown that by inducing a magnetic resonance, the proposed structure confines electromagnetic energy at the first- and third-order resonances. This energy mainly dissipates in the dielectric spacer, causing a near-unity absorption. By using the super cell with four rings or nine rings, we designed and fabricated the broadband MMs absorbers. It was found that the bandwidth (with absorption over 90%) is 1.3 GHz and 2.17 GHz when the unit cell is four- and nine-rings, respectively. The influence of geometry parameters was also investigated. The results show that the absorption frequency and the intensity was strongly dependent on the structure parameters such as radius of rings, the dielectric thickness. The experiment results of one-ring, four-rings and nine-rings shaped structure are in good agreement with the simulation ones. Finally, by scaling down the unit-cell size, the THz-MAs and broadband MMs absorber are realized in the THz frequency based on the third-order resonance. Our results are foundation for the development of the new generation of nanotechnology-enabled solutions operating across the entire electromagnetic spectrum such as broad-bandwidth, polarization control devices, data processing, sensors, optical devices and energy conversion devices.

Acknowledgment. This research was funded by Vietnam National Foundation for Science and Technology Development (NAFOSTED) under Grant No. ‘‘103.99-2018.35’’; and by the Institute of Materials Science, Vietnam Academy of Science and Technology under Grant No. HTCBT.05/20-20.

REFERENCES

1. Veselago V. G. - The electrodynamics of substances with negative ε and μ, Sov. Phys. Usp. **10** (1968) 509.
2. Smith D. R., Padilla W. J., Vier D. C., Nemat-Nasser S. C., and Schultz S. - Composite medium with simultaneously negative perme-ability and permittivity, Phys. Rev. Lett. **84** (2000) 4184.
3. Hien N. T., Tung B. S., Sen Y., Vandenbosch G. A. E., Lievens P., Lam V. D. and Janssens E. - Broadband negative refractive index obtained by plasmonic hybridization in metamaterials, App. Phys. Lett. **109** (2016) 221902.
4. Hien N. T., Hai L. D., Tung B. S., Khuyen B. X., Ca N. X., Lam V. D. - Plasmonic hybridization in symmetric metamaterial for broadband negative refractive index: simulation, experiment and characterization, J. Phys. D: Appl. Phys. **53** (2020) 175501.
5. Shuaishuai T., Chunyu R. and Weipeng T. - High-transmission negative refraction in the gradient space-coiling metamaterials, Appl. Phys. Lett. **114** (2019) 204101.
6. Pendry J. B. - Negative refraction makes a perfect lens, Phys. Rev. Lett. **85** (2000) 3966.
7. Schurig D., Mock J. J., Justice B. J., Cummer S. A., Pendry J. B., Starr A. F., and Smith D. R. - Demonstration of a metamaterial electromagnetic cloak at microwave frequencies, Science **314** (2006) 977.
8. Pendry J. B., Schurig D., Smith D. R. - Controlling electromagnetic fields, Science **312** (2006) 1780.
9. Hwang J. S., Tung B. S. and Lee Y. P. - Electromagnetically-induced Transparency in Metamaterials for the Potential Applications, J. Korean Phys. Soc. **72** (2018) 1491.

10. Kun R., Yumeng H., Xiaobin R., Ying Z., Qun H., Liedong W. and Maojun X. - Dynamically tunable multi-channel and polarization-independent electromagnetically induced transparency in terahertz metasurfaces, J. Phys. D: Appl. Phys. **53** (2020) 122593.
11. Kevin Pichler, Matthias Kuhmayer, Julian Bohm, Andre Brandstotter, Philipp Ambichi, Ulrich Kuhl and Stefan Rotter - Random anti-lasing through coherent perfect absorption in a disordered medium, Nature **567** (2019) 351.
12. Singh G., Sheokand H., Chaudhary K., Srivastava K. V., Ramkumar J. and Ramakrishna S. A. - Fabrication of non-wettable wearable textile based metamaterial microwave absorber, J. Phys. D: Appl. Phys. **52** (2019) 385304.
13. Khuyen B. X., Tung B. S., Tung N. T., Hien N. T., Kim Y. J., Chen L. Y., Lee Y. P., Linh P. T. and Lam V. D. - Realization for dual-band high-order perfect absorption, based on metamaterial, J. Phys. D: Appl. Phys. **53** (2020) 105502.
14. Liu X., Tyler T., Starr T., Starr A., Jokerst N. M. and Padilla W. J. - Taming the Blackbody with Infrared Metamaterials as Selective Thermal Emitters, Phys. Rev. Lett. **107** (2011) 045901.
15. Chang Y. C., Wang C. M., Abbas M. N., Shih M. H. and Tsai D. P. - T-shaped plasmonic array as a narrow-band thermal emitter or biosensor, Opt. Express **17** (2009) 13526.
16. Lai J. J., Liang H. F., Peng Z. L., Yi X. and Zhai X. F. - MEMS integrated narrow band infrared emitter and detector for infrared gas sensor, J. Phys.: Conf. Ser. **276** (2011) 012129.
17. Liu N., Mesch M., Weiss T., Hentschel M., Giessen H. - Infrared Perfect Absorber and Its Application As Plasmonic Sensor, Nano Lett. **10** (2010) 2342.
18. Chan W. L., Chen H. T., Taylor A. J., Brenner I., Cich M. J. and Mittleman D. M. - A spatial light modulator for terahertz beams, Appl. Phys. Lett. **94** (2009) 213511.
19. Bienz E. F. - Thermal camouflage, US Patent (1979) 4142015.
20. Singh P., Korolev K. A., Afsar M. N. and Sonkusale S. - Single and dual band 77/95/110 GHz metamaterial absorbers on flexible polyimide substrate, Appl. Phys. Lett. **99** (2011) 264101.
21. Landy N. I., Sajuyigbe S., Mock J. J., Smith D. R., Padilla W. J. - Perfect Metamaterial Absorber, Phys. Rev. Lett. **100** (2008) 207402.
22. Cuong T. M., Hai P. V., Hung H. T., Thuy N. T., Tung D. H., Khuyen B. X., Tung B. S., Tuyen L. D., Linh P. T., Lam V. D. - Broadband microwave coding metamaterial absorbers, Sci. Rep. **10** (2020) 1810.
23. Niesler F. B. P., Gansel J. K., Fischbach S., Wegener M. - Metamaterial metal-based bolometers, Appl. Phys. Lett. **100** (2012) 203508.
24. Lii C., Qiu J., Ou J. Y., Liu Q. H., Zhu J. - High-Sensitivity Refractive Index Sensors Using Coherent Perfect Absorption on Graphene in the Vis-NIR Region, ACS Appl. Nano Mater. **2** (2019) 3231.
25. Zhang H., Feng L., Liang Y. and Xu T. - An ultra-flexible plasmonic metamaterial film for efficient omnidirectional and broadband optical absorption, Nanoscale **11** (2019) 437.

26. Aydin K., Ferry V. E., Briggs R. M., Atwater H. A. - Broadband polarization-independent resonant light absorption using ultrathin plasmonic super absorbers, Nat. Commun. **2** (2011) 517.
27. Cheng Y. Z., Wang Y., Nie Y., Gong R. Z., Xiong X., Wang X. - Design, fabrication and measurement of a broadband polarization-insensitive metamaterial absorber based on lumped elements, J. Appl. Phys. **111** (2012) 044902.
28. Wang T., Lizhi Q., Lingfei Q., Zhang Y., Zhang H. and Cao M. - Tunable broadband terahertz metamaterial absorber using multi-layer black phosphorus and vanadium dioxide, J. Phys. D: Appl. Phys. **53** (2020) 122677.
29. Chen S., Cheng H., Yang H., Li J., Duan X., Gu C., Tian J. - Polarization insensitive and omnidirectional broadband near perfect planar metamaterial absorber in the near infrared regime, Appl. Phys. Lett. **99** (2011) 253104.
30. Wakatsuchi H., Greedy S., Christopoulos C., Paul J. - Customised broadband metamaterial absorbers for arbitrary polarisation, Opt. Express **18** (2010) 22187.
31. Ding F., Cui Y., Ge X., Jin Y., He S. - Ultra-broadband microwave metamaterial absorber Appl. Phys. Lett. **100** (2012) 103506.
32. Tao H., Bingham C. M., Strikwerda A. C., Pilon D., Shrekenhamer D., Landy N. I., Fan K., Zhang X., Padilla W. J. and Averitt R. D. - Highly flexible wide angle of incidence terahertz metamaterial absorber: Design, fabrication, and characterization, Phys. Rev. B **78** (2008) 241103.
33. Tung N. T., Thuy V. T. T., Park J. W., Rhee J. Y., and Lee Y. P. - Left-handed transmission in a simple cut-wire pair structure, Jour. Appl. Phys. **107** (2010) 023530.
34. Viet D. T., Tung N. T., Hien N. T., Lee Y. P., Tung B. S. and Lam V. D. - Multi-plasmon resonances supporting the negative refractive index in “single-atom” metamaterials, J. Nonlinear Opt. Phys. Mater. **21** (2012) 1250019.
35. Ye Y. Q., Jin Y. and He S. - Omnidirectional, polarization-insensitive and broadband thin absorber in the terahertz regime, J. Opt. Soc. Am. **27** (2010) 498.
36. Tao H., Bingham C. M., Pilon D., Fan K., Strikwerda A. C., Shrekenhamer D., Padilla W. J., Zhang X. and Averitt R. D. - A dual band terahertz metamaterial absorber, J. Phys. D **43** (2010) 225102.
37. Watts C. M., Liu X. and Padilla W. J. - Metamaterial Electromagnetic Wave Absorbers, Adv. Mater. **24** (2012) 98.
38. Hien N. T., Tung B. S., Tuan N. T., Tung N. T., Lee Y. P., An N. M. and Lam V. D. - Metamaterial-based perfect absorber: polarization insensitivity and broadband, Adv. Nat. Sci.: Nanosci. Nanotechnol. **5** (2014) 025013.
39. Nie P., Zhu D., Cui Z., Qua F., Lina L., Wang Y. - Sensitive detection of chlorpyrifos pesticide using an all-dielectric broadband terahertz metamaterial absorber, Sens. Actuators B Chem. **15** (2020) 127642.